

DVIS-DAQ: Improving Video Segmentation via Dynamic Anchor Queries

Yikang Zhou^{1*}, Tao Zhang^{1,2 *}, Shunping Ji¹,
Shuncheng Yan², and Xiangtai Li^{2 †}

¹ Wuhan University

² Skywork AI

zhang_tao@whu.edu.cn, zhoyik@whu.edu.cn, xiangtai94@gmail.com

Project page: https://zhang-cao-whu.github.io/projects/DVIS_DAQ

Abstract. Modern video segmentation methods adopt object queries to perform inter-frame association and demonstrate satisfactory performance in tracking continuously appearing objects despite large-scale motion and transient occlusion. However, they all underperform on newly emerging and disappearing objects that are common in the real world because they attempt to model object emergence and disappearance through feature transitions between background and foreground queries that have significant feature gaps. We introduce Dynamic Anchor Queries (DAQ) to shorten the transition gap between the anchor and target queries by dynamically generating anchor queries based on the features of potential candidates. Furthermore, we introduce a query-level object Emergence and Disappearance Simulation (EDS) strategy, which unleashes DAQ’s potential without any additional cost. Finally, we combine our proposed DAQ and EDS with DVIS [71] to obtain DVIS-DAQ. Extensive experiments demonstrate that DVIS-DAQ achieves a new state-of-the-art (SOTA) performance on five mainstream video segmentation benchmarks. Code and models are available at <https://github.com/SkyworkAI/DAQ-VS>.

Keywords: Video segmentation · Dynamic anchor design · Universal segmentation

1 Introduction

Video segmentation aims at simultaneously identifying, segmenting, and tracking all objects of interest within a video [24, 47, 65, 66], which has many applications, including autonomous driving, video editing, content analysis, and video understanding [5, 45]. Modern video segmentation methods [18, 21, 23, 28, 33, 60, 68, 71, 72] utilize object queries to perform cross-frame association and achieve remarkable performance. Despite large-scale motion and transient occlusion, these methods yield satisfactory results in continuously appearing objects.

* The first two authors contribute equally. This work was performed when Tao Zhang was an Intern at Skywork AI. † Project Leader.

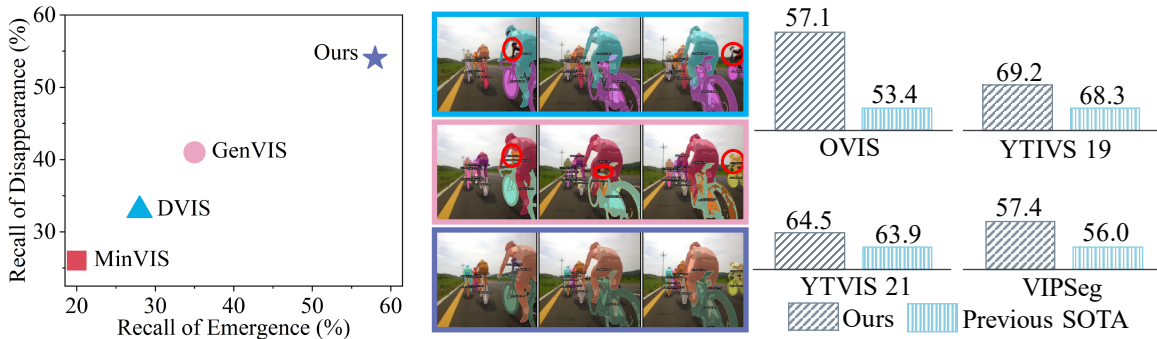


Fig. 1: The preliminary experiments and our results. We analyze current query-based video segmentation methods’ capabilities in handling objects’ emergence and disappearance within videos. The scatter plot on the left illustrates the recall ratios for newly emerging and disappearing video objects on a subset of the BDD [69] dataset. The visual comparison is presented in the middle. The top two rows output from DVIS [71] and GenVIS [21], respectively. And the bottom row output from our method. The poor performance of previous methods on new emergence detection and disappearance filtering is highlighted by a red circle. On the right side, our method outperforms the current SOTA on mainstream video segmentation datasets.

However, these query-based methods exhibit a notable limitation: they tend to underperform when dealing with *newly emerging* or *disappearing objects*, even with recent state-of-the-art (SOTA) methods [21, 71]. As shown in the left part of Fig. 1, these methods only achieve less than 45% recall ratio on emerging and disappearing objects. As illustrated in the middle part of Fig. 1, they often fail to detect newly emerging objects. And they may incorrectly track a different, similar object when the original object disappears. Given that many objects appear and disappear over time in real-world long videos, it is imperative to improve these methods to handle objects’ emergence and disappearance more effectively, thereby meeting the requirements of real-world application requirements.

A natural question arises: "What causes the huge performance gap between continuously appearing objects and emerging/disappearing objects?" We argue the answer lies in the unreasonable anchor queries used in current methods. As shown in Fig. 2, SOTA query-based methods [21, 23, 71, 72] use the background query as the anchor query and model the object’s emergence and disappearance as a feature transition between the background and foreground query. However, a significant transition gap between background and foreground queries poses considerable challenges during training. To illustrate, consider emergence as an example. It is difficult for the model to learn how to transform a background anchor query into a foreground query without any semantic similarity. Consequently, the model may fail to transform and retain the background anchor query, resulting in missing newly emerging objects. Similarly, for disappearing objects, the model may prefer to incorrectly transform their query into another object’s query with more semantic similarity.

In this paper, we address this challenge by introducing **Dynamic Anchor Queries (DAQ)** mechanism to detect the emergence and disappearance of ob-

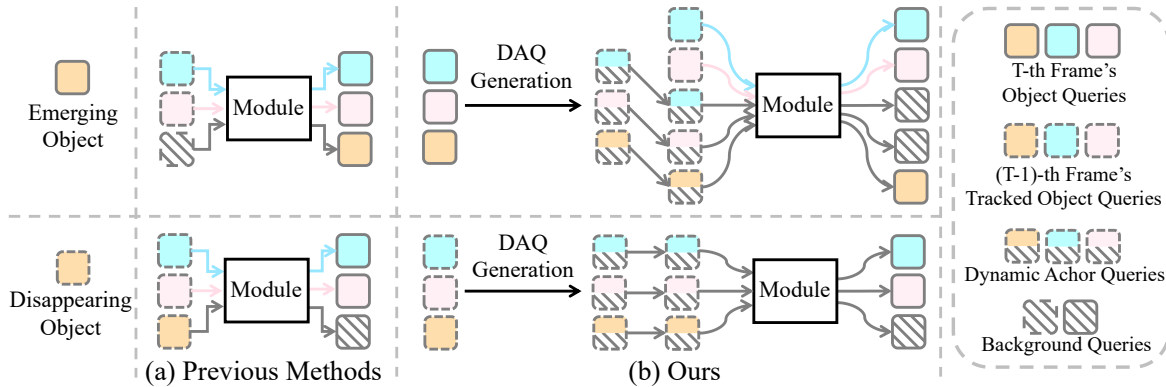


Fig. 2: The process of handling newly emerging and disappearing objects in different methods. Unlike previous approaches that treat appearing, disappearing, and tracked objects equally, our method dynamically generates anchor queries for emergence and disappearance based on candidate objects’ features to effectively shorten the transition gap.

jects. As illustrated on the right side of Fig. 2, we regard all objects segmented in the current frame as potential candidates for newly emerging objects. We dynamically generate emergence anchor queries based on the features of these candidates to reduce the transition gap significantly. In particular, we designate all tracked objects as candidates for disappearing objects and generate disappearance anchor queries dynamically using their features. These emergence and disappearance anchor queries and the representations of tracked objects are collectively inputted into the tracker to identify the objects of interest in the current frame. Objects identified by the emergence anchor queries are classified as newly appeared, while those pinpointed by the disappearance anchor queries are recognized as having disappeared, prompting their removal. The remaining queries are responsible for tracking objects present across both past and current frames.

The proposed DAQ mechanism enhances the network’s ability to handle the emergence and disappearance of objects. However, emergence and disappearance events are rare in existing video segmentation datasets. To further leverage the capabilities of DAQ, we propose a training time simulation strategy for the emergence and disappearance of objects, termed **Emergence and Disappearance Simulation (EDS)**. This strategy simulates emergence and disappearance events by removing high-level object queries. We mimic object emergence by randomly eliminating some object queries propagated from the previous frame. Likewise, we simulate object disappearance by removing some of the current frame’s object queries. Our simple yet effective simulation strategy generates numerous instances of object emergence and disappearance during training, thereby enabling comprehensive training of the DAQ mechanism and maximizing its potential.

To verify the effectiveness of our proposed DAQ mechanism and EDS strategy, we integrate them into the current SOTA method, DVIS [71], to construct the DVIS-DAQ. As shown in the right part of Fig. 1, our proposed DVIS-DAQ achieves new SOTA performance on five mainstream video segmentation benchmarks and significantly outperforms previous SOTA methods.

In summary, our main contributions are as follows:

1. We have found that current query-based methods fall short in managing objects’ emergence and disappearance due to the considerable transition gap between foreground and background queries. We propose a Dynamic Anchor Queries (DAQ) mechanism to address this challenge. The DAQ mechanism dynamically generates anchor queries for objects’ emergence and disappearance, thereby shortening the gap and effectively overcoming the challenge.
2. To further unleash the potential of the DAQ mechanism, we introduce the Emergence and Disappearance Simulation (EDS) strategy. This straightforward and efficient approach amplifies the number of emergence and disappearance cases, thereby ensuring comprehensive training of the DAQ.
3. We enhance the SOTA video segmentation method DVIS by integrating our proposed DAQ mechanism and EDS strategy, resulting in DVIS-DAQ. With extensive experiments on five video segmentation benchmarks, DVIS-DAQ achieves new SOTA performance on all benchmarks. We further present detailed ablation studies to verify the effectiveness of each component.

2 Related Work

Video Instance Segmentation (VIS). Earlier works [35, 66, 67] extend image instance segmentation methods by adding tracking heads and learning the feature association. With the rise of vision transformer [8, 16, 54], current SOTA video instance methods [10, 18, 22, 23, 28, 33, 37, 54, 59, 60, 68] adopt query-based designs. In particular, Video K-Net [34] and IDOL [60] directly learn the query association embeddings via contrastive learning. After that, association-based methods [23, 33, 37, 60, 66, 68], accomplish the tracking of video targets between adjacent frames or adjacent video clips through object matching. Meanwhile, several models [10, 22, 59] directly predict 3D volumes of video instances across times in a semi-online manner. On the other hand, propagation-based methods [18, 21, 28, 71] delegate the tracking problem to the transformer decoder. They take the object queries outputted from the previous frame or video clip as input and iteratively optimize them to segment the objects in the current frame. Note that these methods can also be applied for video panoptic segmentation (VPS) and video semantic segmentation (VSS) tasks [24, 39, 40, 48, 55, 78] by adding queries for segmenting the stuff. However, both poorly handle challenges such as new-emerging objects and target disappearance. Our approach improves the model’s ability to address these challenges by employing dynamic anchor queries to manage the emergence and disappearance of objects.

Universal Video Segmentation. Current efforts in the field of video segmentation directly draw upon the design of universal image segmentation models [10, 12, 13, 53, 56, 64, 73] to develop universal video segmentation models [1, 26, 30, 31, 33, 34, 58, 71], achieving comparable or even superior performance to specialized video segmentation methods. Video K-Net [34] and TubeFormer [26] are the first to unify all three video segmentation tasks. TarVIS [1] extends the concept of mask classification from image segmentation to video segmentation,

accomplishing universal video segmentation via one shared model. DVIS [71] receives frame object query outputs from Mask2Former [10] for universal video segmentation. Recently, several works [32, 62] unified both image and video segmentation in one model. However, these methods are still unaware of object emergence and disappearance problems, which are significant for long videos.

Video Object Tracking. Object tracking [3, 7, 14, 17, 42, 43, 50, 51, 63, 70, 74, 75] is a crucial task in VIS and VPS [4, 19, 24, 25, 29, 76], and many works adopt the tracking-by-detection paradigm [6, 27, 38, 46, 52, 57, 61, 77]. These methods divide the task into two sub-tasks, where an object detector first detects objects and then associates them using a tracking algorithm. Recent works [2, 15, 44, 49] also perform clip-wise segmentation and tracking. However, the former [15, 44] only focuses on single-object mask tracking, while the latter [49] considers global tracking via clip-level matching. Our work belongs to mask-based tracking, which is orthogonal to these existing tracking methods.

3 Method

3.1 Preliminary

Query-based Video Segmentation Formulations. Modern mainstream video segmentation methods [21, 33, 60, 71, 72] rely on queries to represent objects and achieve cross-frame association of objects. Here, we summarize current query-based video segmentation methods with the following formulation:

$$Q_{Seg}^T = \mathcal{S}(\mathcal{I}^T), \quad Q^T = \mathcal{A}(Q^{T-1}, Q_{Seg}^T), \quad \mathcal{M}^T, \mathcal{C}^T = \mathcal{D}(Q^T). \quad (1)$$

First, a segmenter \mathcal{S} extracts query representations of objects Q_{Seg}^T from a single-frame image. Then, an association component \mathcal{A} establishes connections between the current frame’s object representations Q_{Seg}^T and Q^{T-1} to obtain associated object representations Q^T . Finally, the object representations Q^T are decoded to obtain predictions of object categories \mathcal{C}^T and segmentation masks \mathcal{M}^T for the current frame. In this pipeline, the association component \mathcal{A} is the most critical and challenging part. Most video segmentation methods focus on designing more efficient association modules.

The current mainstream association modules \mathcal{A} can be divided into association-based [23, 33, 60, 68] and propagation-based [21, 71, 72] pipelines. They both model object emergence as a transition from background queries to foreground queries and model disappearance as a transition from foreground queries to background queries. Specifically, we can split Q ($Q = \{Q_{Bg}, Q_{Fg}\}$) into Q_{Fg} and Q_{Bg} , and the tracking of continuously appearing objects, newly emerging objects, and disappearing objects can be described as follows:

$$Cont : Q_{Fg}^{T-1} \rightarrow Q_{Fg}^T, \quad Emg : Q_{Bg}^{T-1} \rightarrow Q_{Fg}^T, \quad Dis : Q_{Fg}^{T-1} \rightarrow Q_{Bg}^T \quad (2)$$

Limitations of the Query-based Methods. We find that current query-based methods [21, 23, 71] perform poorly on objects that emerge and disappear in the

middle of a video, as shown in Fig. 1. For emerging objects, SOTA methods often miss detecting them. For disappearing objects, SOTA methods frequently fail to recognize that the object has disappeared and may incorrectly segment another object. We quantitatively analyzed the recall ratios of emerging and disappearing objects in preliminary experiments using several SOTA methods. We found that the recall ratios of emerging and disappearing objects are very low (below 45%) for these methods, as shown in Fig. 1.

Thorough Analysis and Our Motivation. Query-based methods have demonstrated satisfactory performance on consistently appearing objects (exceeding 60 AP on the YouTube-VIS [66]), but they exhibit poor performance on newly emerging and disappearing objects. As depicted in Fig. 2 and Eq. 2, in current query-based methods, there is a significant disparity in the modeling formulation between newly emerging or disappearing objects and consistently appearing objects. The former poses more challenges because of the significant feature gap in the transition between foreground and background queries. In this work, we dynamically generate anchor queries for newly emerging and disappearing objects, resulting in a lower feature transition gap than the background query. We term the background query used in previous methods as Static Anchor Query (SAQ), the query of continuously appearing objects as Continuously Tracked Query (CTQ), and our proposed dynamically generated anchor query as Dynamic Anchor Query (DAQ). We use our proposed DAQ to replace the SAQ to address the challenge above. The details of the DAQ will be introduced in Sec. 3.2.

Furthermore, we observed that only less than 20% of samples contain object emergence and disappearance in the existing datasets [39, 47, 66], including the most challenging OVIS [47] dataset. Therefore, to fully unleash the potential of our proposed DAQ, we introduce a simple yet effective query-level object emergence and disappearance simulation strategy, which will be detailed in Sec. 3.3.

3.2 Dynamic Anchor Queries

The key idea of DAQ is to dynamically generate anchor queries using the features of candidate objects that may emerge or disappear, thereby reducing the gap between anchor queries and the target queries (the queries of actual newly emerging or disappearing objects). DAQ allows the network to easily transform anchor queries to target queries and effectively handle object emergence and disappearance.

In this subsection, we introduce how to design and utilize Dynamic Anchor Queries (DAQ) to address the challenges mentioned above. First, we explain how the DAQ for newly emerging and disappearing objects are generated. Then, we explore how to make minor adjustments to the current query-based tracker to accommodate our proposed DAQ.

Dynamic Anchor Queries for Emergence. When processing the T^{th} frame of a video, we consider all objects appearing in the current frame as candidates for newly emerging objects. The dynamic anchor queries for emergence DAQ_{Emg} are naturally generated based on the features of these candidates. As shown in

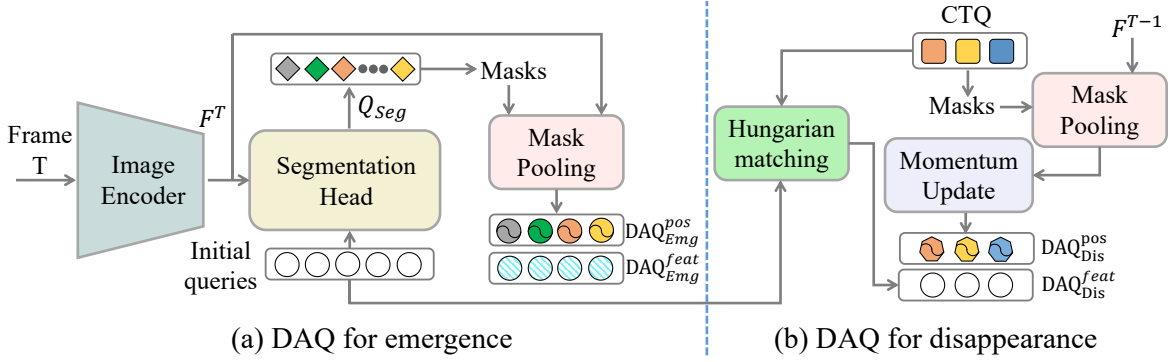


Fig. 3: Generation of dynamic anchor queries. F^T represents the image feature of the T^{th} frame. Symbols Emg and Dis denote emergence and disappearance. Symbols $feat$ and pos indicate feature and positional embedding, respectively.

Fig. 3 (a), DAQ_{Emg} consists of two parts: query feature DAQ_{Emg}^{feat} and query positional embedding DAQ_{Emg}^{pos} . The query feature DAQ_{Emg}^{feat} is a learnable embedding shared by all dynamic anchor queries. The query positional embedding DAQ_{Emg}^{pos} is obtained using the appearance features F_{mask}^T of the candidates through simple Mask-Pooling:

$$F_{mask}^T = \text{MLP}(\text{MaskPooling}(F^T, \mathcal{M}^T)), \quad (3)$$

where F^T represents the image feature of the $T - th$ frame, and \mathcal{M}^T represents the segmentation masks of the candidates outputted by the segmenter.

Dynamic Anchor Queries for Disappearance. When processing the T^{th} frame, we consider all currently tracked objects as candidates for disappearing objects. Similar to the dynamic anchor queries for emergence, the DAQ_{Dis} for disappearing objects are naturally generated based on the features of these candidates. As shown in Fig. 3 (b), the DAQ_{Dis} also consists of query feature DAQ_{Dis}^{feat} and query positional embedding DAQ_{Dis}^{pos} . We use the candidates' momentum-weighted appearance features \bar{F}_{mask}^T as the query positional embedding DAQ_{Dis}^{pos} . The momentum-weighted function follows CTVIS [68]:

$$\bar{F}_{mask}^T = (1 - \beta)\bar{F}_{mask}^{T-1} + \beta F_{mask}^T \quad (4)$$

$$\beta = \max\left(0, \frac{1}{T} \sum_{t=1}^{T-1} \text{cosine}(F_{mask}^t, F_{mask}^T)\right) \quad (5)$$

Since the disappearance of an object needs to be modeled as a transition from an anchor query to a background query, to reduce the transition gap, we use initial queries of segmenter as the query feature DAQ_{Dis}^{feat} . Specifically, for each query feature, we match the closest one from the initial queries of the segmenter based on cosine similarity.

Continuously Tracked Queries. We also assign query positional embedding CTQ^{pos} for continuously tracked queries (CTQ) to maintain the format consis-

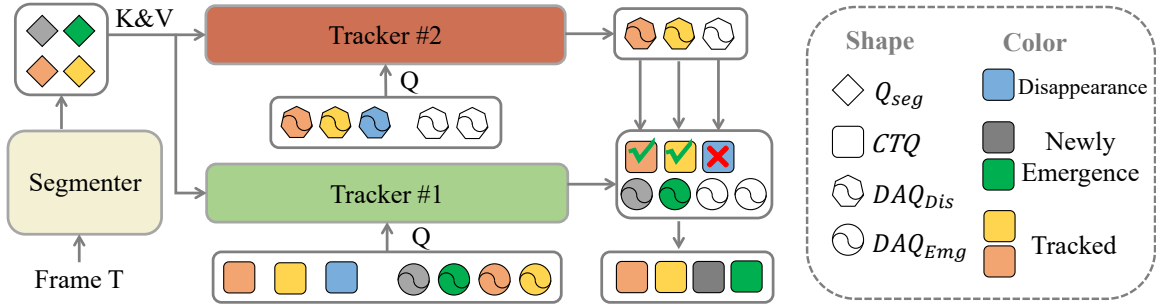


Fig. 4: Tracker with dynamic anchor queries. Q_{seg} represents the query output of segmenter. CTQ and DAQ stand for continuously tracked and dynamic anchor queries, respectively. Symbols Emg and Dis denote emergence and disappearance.

tency with dynamic anchor queries. We use the momentum-weighted appearance feature of the tracked objects as CTQ^{pos} , the same process as Eq. 3, 4, and 5.

Incorporating Dynamic Anchor Queries into a Tracker. As depicted in Fig. 4, we can seamlessly integrate DAQ into mainstream propagation-based trackers [21, 71], requiring no alterations to the tracker’s network architecture. We instantiate two trackers: Tracker 1, which takes CTQ and DAQ_{Emg} as inputs and is responsible for tracking continuously appearing and newly emerging objects, and Tracker 2, which receives DAQ_{Dis} along with several learnable background embeddings as inputs and identifies disappearing objects in the current frame. It’s important to note that the SoftMax function in Tracker 2 operates along the Q-dimension to prevent multiple dynamic anchor queries from segmenting the same object. Through this pipeline, we can effectively and reasonably manage and model the emergence and disappearance of objects. Despite introducing an additional tracker, it’s worth highlighting that the computational overhead is minimal, constituting less than 2% of the overall computational cost [71], as processing occurs solely at the query level rather than on dense image features.

3.3 Emergence and Disappearance Simulation

As shown in Fig. 5, when using DAQ, it is possible to simulate object emergence and disappearance separately by removing parts of CTQ and Q_{Seg} , respectively. We term this simple yet efficient simulation strategy as Emergence and Disappearance Simulation (EDS), which includes Emergence Simulation (ES) and Disappearance Simulation (DS). EDS can simulate numerous object emergence and disappearance cases during training without introducing additional costs, allowing the network to be fully trained and unleashing the potential of DAQ.

New Emergence Simulation. As shown in Fig. 5 (a), taking the green object as an example, we can simulate it as an emerging object by removing its corresponding query from CTQ. At this point, this green object is not present in CTQ but exists in the current frame, consistent with the state of a real newly emerged object colored in gray. Then, the Tracker needs to transition the corresponding anchor query from DAQ_{Emg} to a foreground query and predict this green object’s segmentation mask and class.

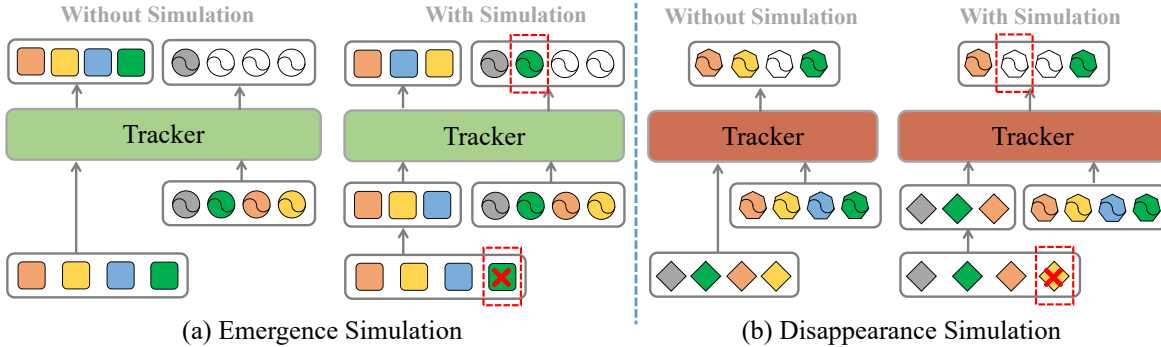


Fig. 5: The pipelines of emergence and disappearance simulation. CTQ, DAQ_{Emg} , DAQ_{Dis} , and Q_{Seg} are represented by rectangles, circles, diamonds, and heptagons, respectively. White indicates the background query transformed from the anchor query. The red rectangles highlight the difference between with and without simulation.

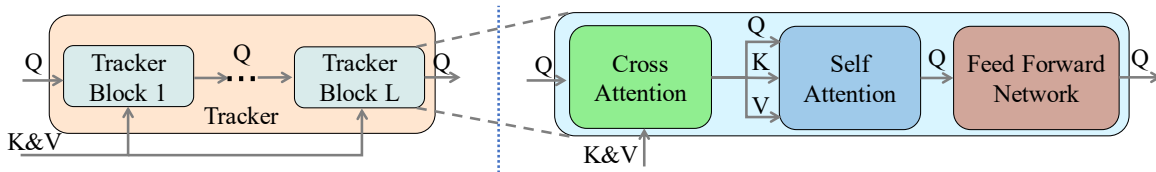


Fig. 6: The architecture of DVIS-DAQ tracker.

Disappearance Simulation. As shown in Fig. 5 (b), taking the yellow object as an example, by removing its corresponding query from Q_{Seg} , we can simulate this object as a disappearing object because the Tracker only detects features from Q_{Seg} through cross-attention to obtain image information. At this point, this blue object is not present in the current frame but exists in the set of tracked objects, consistent with the state of a real disappearing blue object. The Tracker needs to transition the corresponding anchor query to a background query and determine the disappearance of this object.

3.4 Overall Architecture

Architecture. Sec. 3.2 details how DAQ is integrated into the current query-based tracker without any requirement for architecture modification. We apply the SOTA video segmentation method DVIS [71] as our baseline and replace the Referring Cross-Attention [71, 72] in its tracker with standard Cross-Attention to achieve a more straightforward and generalizable structure shown in Fig. 6. We then integrated DAQ into this simplified tracker, resulting in our architecture, DVIS-DAQ.

Objective Function. Our objective function differs from DVIS [71]. We maintain the historical matching relationship between the predictions of CTQ and ground truth for continuously tracked objects and remove the matched items from the ground truth. For newly emerging and disappearing objects, since DAQ is dynamically generated based on the features of candidates (refer to Sec. 3.2),

Table 1: Results on the val set of OVIS and YouTube-VIS 2019 & 2021. † denotes with the offline refiner proposed by [71]. The VIT-L [16] is pre-trained by DINOv2 [41] and uses VIT-Adapter [9] to obtain multiscale features.

Method	Backbone	OVIS			YT-VIS 2019			YT-VIS 2021		
		AP	AP ₇₅	AR ₁₀	AP	AP ₇₅	AR ₁₀	AP	AP ₇₅	AR ₁₀
MinVIS [23]	R50	25.0	24.0	29.7	47.4	52.1	55.7	44.2	48.1	51.7
CTVIS [68]	R50	35.5	34.9	41.9	55.1	59.1	63.2	<u>50.1</u>	<u>54.7</u>	59.5
GenVIS [21]	R50	35.8	36.2	39.6	50.0	54.6	59.7	47.1	51.5	54.7
DVIS [71]	R50	30.2	30.5	37.3	51.2	57.1	59.3	46.4	49.6	53.5
DVIS† [71]	R50	33.8	33.5	39.5	52.3	58.2	60.4	47.4	51.6	55.2
DVIS++ [72]	R50	37.2	37.3	42.9	55.5	<u>60.1</u>	<u>62.6</u>	50.0	54.5	<u>58.4</u>
DVIS+++† [72]	R50	<u>41.2</u>	<u>40.9</u>	<u>47.3</u>	-	-	-	-	-	-
DVIS-DAQ	R50	38.7	37.6	45.2	<u>55.2</u>	61.9	63.7	50.4	55.0	57.6
DVIS-DAQ†	R50	43.5	43.8	49.1	-	-	-	-	-	-
MinVIS [23]	Swin-L	39.4	41.3	43.3	61.6	68.6	66.6	55.3	62.0	60.8
CTVIS [68]	Swin-L	46.9	47.5	52.1	65.6	72.2	70.4	61.2	68.8	65.8
GenVIS [21]	Swin-L	45.2	48.4	48.6	64.0	68.3	69.4	59.6	65.8	65.0
DVIS [71]	Swin-L	45.9	48.3	51.5	63.9	70.4	69.0	58.7	66.6	64.6
DVIS† [71]	Swin-L	48.6	50.5	53.8	64.9	72.7	70.3	60.1	68.4	65.7
DVIS++ [72]	VIT-L	49.6	55.0	54.6	67.7	75.3	<u>73.7</u>	62.3	70.2	68.0
DVIS+++† [72]	VIT-L	53.4	<u>58.5</u>	58.7	<u>68.3</u>	<u>76.1</u>	73.4	<u>63.9</u>	<u>71.5</u>	<u>69.5</u>
DVIS-DAQ	Swin-L	49.5	51.7	54.9	65.7	73.6	70.7	61.1	68.2	66.6
DVIS-DAQ	VIT-L	<u>53.7</u>	58.2	<u>59.5</u>	<u>68.3</u>	<u>76.1</u>	73.5	62.4	70.8	68.0
DVIS-DAQ†	VIT-L	57.1	62.9	62.3	69.2	76.8	75.5	64.5	72.4	70.7

we assign the remaining ground truth to DAQ based on the matching relationship between candidates and the remaining ground truth. Following this process, we obtain the matching relationship $\{(i, \sigma(i)) | i \in [1, M]\}$ between ground truth and predictions, M is the number of ground truth. The not-matched predictions are assigned with the background class and an empty segmentation mask. Then, the loss between matched prediction-label pairs $(\mathcal{P}, \mathcal{G})$ can be calculated following the Mask2Former [11]:

$$\mathcal{L}(\mathcal{P}, \mathcal{G}) = \lambda_{cls} \mathcal{L}_{cls}(\mathcal{P}, \mathcal{G}) + \lambda_{dice} \mathcal{L}_{dice}(\mathcal{P}, \mathcal{G}) + \lambda_{bce} \mathcal{L}_{bce}(\mathcal{P}, \mathcal{G}) \quad (6)$$

Here, \mathcal{L}_{cls} represents the classification loss term, implemented using Cross Entropy Loss. \mathcal{L}_{dice} and \mathcal{L}_{bce} denote the segmentation loss terms, implemented respectively using Dice loss and Binary Cross Entropy loss.

4 Experiment

4.1 Datasets and Metrics

We conduct experiments on five mainstream video segmentation benchmarks, including OVIS [47], Youtube-VIS 2019 & 2021 & 2022 [66], and VIPSeg [39]. We employ AP and AR as evaluation metrics for the VIS datasets following [66]. We

Table 2: Results on the validation sets of YouTube-VIS 2022 and VIPSeg. AP^L refers to the AP on the long video set. VPQ^{Th} and VPQ^{St} refer to the VPQ on the "thing" objects and the "stuff" objects, respectively.

Method	Backbone	YT-VIS 2022			VIPSeg			
		AP^L	AP_{75}^L	AR_{10}^L	VPQ	VPQ^{Th}	VPQ^{St}	STQ
MinVIS [23]	R50	23.3	19.3	28.0	-	-	-	-
TarVIS [1]	R50	-	-	-	33.5	39.2	28.5	43.1
DVIS [71]	R50	<u>31.6</u>	<u>37.0</u>	<u>36.3</u>	39.4	38.6	40.1	36.3
DVIS++ [72]	R50	37.2	40.7	44.6	<u>41.9</u>	<u>41.0</u>	42.7	38.5
DVIS-DAQ	R50	<u>34.6</u>	35.5	<u>41.1</u>	42.1	41.7	<u>42.5</u>	<u>39.3</u>
MinVIS [23]	Swin-L	33.1	33.7	36.6	-	-	-	-
TarVIS [1]	Swin-L	-	-	-	48.0	<u>58.2</u>	39.0	52.9
DVIS [71]	Swin-L	<u>39.9</u>	<u>42.6</u>	<u>44.9</u>	54.7	54.8	<u>54.6</u>	47.7
DVIS++ [72]	VIT-L	37.5	39.4	43.5	<u>56.0</u>	58.0	54.3	49.8
DVIS-DAQ	VIT-L	42.0	43.0	48.4	57.4	60.4	54.7	<u>52.0</u>

utilize Video Panoptic Quality (VPQ) and Segmentation and Tracking Quality (STQ) for the VPS datasets as evaluation metrics following [24,39]. More detailed settings can be found in the supplementary file.

4.2 Main Experiments

Performance on OVIS dataset. The OVIS dataset presents more challenging cases, such as occlusion, fast motion, and complex motion trajectories. We present the quantitative evaluation results in Tab. 1. When using ResNet-50 [20] as the backbone, our method achieves an AP of 38.7 and 43.5 with the off-line refiner, surpassing all existing methods. Compared to the current SOTA DVIS++ [72], our method shows an improvement of 1.5 AP (38.7 vs. 37.2) and 2.3 AP (43.5 vs. 41.2) with the offline refiner. When employing a larger backbone, our method achieves even more significant improvements. With Swin-L [36] as the backbone, our method outperforms DVIS [71] by 3.6 AP (49.5 vs. 45.9). When using VIT-L [16] as the backbone, our method surpasses DVIS++ by 4.1 AP (53.7 vs. 49.6). Notably, our DVIS-DAQ even outperforms DVIS++ with the offline refiner (53.7 vs. 53.4), while DVIS-DAQ with the offline refiner has reached 57.1 AP. These quantitative results demonstrate that our DAQ design significantly enhances the capability of query-based video segmentation methods in processing complex scenes with many object emergence and disappearances.

Performance on Youtube-VIS 2019 & 2021 datasets. The videos in these two datasets are relatively short and feature simple scenes. As shown in Tab. 1, when using ResNet-50 as the backbone, our method achieves a 4.0 AP improvement compared to the baseline DVIS on the YTVIS 2019 and 2021 datasets. When using VIT-L as the backbone, we achieve comparable performance with DVIS++. When using the offline refiner, we outperform DVIS++ by 0.9 AP and 0.6 AP on the YTVIS 2019 and 2021 datasets.

Performance on Youtube-VIS 2022 dataset. Youtube-VIS 2022 has been expanded with 71 long videos based on the 2021 version. Therefore, we only report the AP^L for the long videos in Tab. 2. When using ResNet-50 as the backbone, DVIS-DAQ outperforms the baseline DVIS with 3.0 AP^L . Our method outperforms DVIS++ with 4.5 AP^L (42.0 vs. 37.5) when using VIT-L as the backbone.

Performance on VIPSeg dataset. VIPSeg is a large-scale video panoptic segmentation dataset containing various real-world scenes and more categories. Tab. 2 presents the performance comparison with SOTA methods. Our method achieves new SOTA performance with both ResNet-50 and VIT-L backbone settings. Our method achieves a VPQ of 42.1 when using ResNet-50 as the backbone, surpassing the baseline DVIS by 2.7 VPQ. With VIT-L as the backbone, our method achieves a VPQ of 57.4, demonstrating a 2.4 VPQ improvement over the previous SOTA DVIS++ in "thing" objects.

4.3 Ablation Studies and Analysis

We perform ablation experiments on the OVIS dataset using the ResNet-50 backbone and 40K training iterations. We use DVIS [71] as the baseline. When aligning the training and testing settings with DVIS++ [72], the baseline achieves an AP of 35.4. More detailed settings are provided in the supplementary materials. Moreover, we also refer the readers for more different architectures using our DAQ in supplementary part.

Effectiveness of DAQ and EDS. Tab. 3a presents the ablation studies about our proposed components. Using emergence dynamic anchor queries alone leads to a performance degradation of 2.1 AP, attributed to insufficient examples of emergence objects for training. When the emergence simulation strategy is used alone, performance drops by 3.1 AP, indicating that the unreasonable anchor design in the previous method [71] makes it difficult for the network to learn to handle object emergence, even with sufficient training cases. When emergence dynamic anchor queries and emergence simulation are used together, the reasonable mechanism and sufficient training cases result in a 1.0 AP improvement compared to the baseline. Disappearing dynamic anchor queries contribute to a performance improvement of 0.2 AP. Introducing the Disappearing Simulation strategy to provide sufficient cases of disappearing objects further increases model performance by 0.5 AP.

Emergence dynamic anchor queries. DAQ comprises query feature embedding and positional embedding. Firstly, we explore different strategies for selecting emergency candidates, and the results are presented in Tab. 3b. When choosing the top 100 object predictions of the segmenter as candidates, with only one shared learnable embedding, we obtain 36.4 AP. Setting the number of candidates to the top 50 and the number of learnable embeddings to 2 brings a performance gain of 0.1 AP. To explore potential new objects fully, we choose the top 100 scheme.

In Tab. 3e, we investigate how to generate corresponding dynamic anchor queries based on the features of emerging candidates. We find that utilizing

Table 3: Ablation studies on our proposed DAQ and other network details.

(a) The main ablation study of the proposed DAQ and EDS. The baseline is the extension of DVIS [71]. EDAQ/DDAQ denotes emergence/disappearance DAQ. ES/DS denotes emergence/disappearance simulation.

EDAQ	ES	DDAQ	DS	AP
				35.4
✓				33.3
	✓			32.3
✓	✓			36.4
✓	✓	✓		36.6
✓	✓	✓	✓	37.1

(e) Generation of emergence DAQ. *SegQ/SegP/AppF* denotes the query feature/positional embedding/appearance feature of the segmenter’s frame object output. *Add/Cat* denotes adding/concatenating the selected features to the query feature of emergence DAQ. *Pos* denotes using the selected feature as the positional embedding of emergence DAQ.

Metric	Feature selection			Feature usage		
	<i>SegQ</i>	<i>SegP</i>	<i>AppF</i>	<i>Add</i>	<i>Cat</i>	<i>Pos</i>
AP	34.8	36.0	36.4	36.0	36.2	36.4

(b) Candidates selection for emergence DAQ. K denotes the number of top-scoring candidates. N denotes the number of learnable embeddings.

K	N	AP
100	1	36.4
50	1	35.9
50	2	36.5
25	4	35.6

(c) Threshold selection for new emergence simulation.

Threshold	AP
0.01	34.2
0.05	34.7
0.10	35.6
0.20	34.5
0.50	33.2

(d) Disappearance simulation. *One*, *Continuous*, and *Random* represent simulating disappearance for an object in a solitary frame, all frames, and randomly selected frames within a video clip, respectively.

Type	AP
One	36.3
Continuous	35.8
Random	37.1

(f) Generation of disappearance DAQ. *Learn* and *Initial SegQ* represent initializing the query feature of disappearance DAQ by using a new learnable embedding and the initial queries of segmenter, respectively. *CTQF/CTQP* represent using the query feature/momentum-weighted appearance feature of tracked objects as the positional embeddings of disappearance DAQ.

Metric	Query feature		Positional embedding	
	<i>Learn</i>	<i>Initial SegQ</i>	<i>CTQF</i>	<i>CTQP</i>
AP	36.5	37.1	36.8	37.1

candidates’ appearance features yields the best results, surpassing the use of positional features and object queries with a hybrid of positional and appearance information by 1.6 AP and 0.4 AP, respectively. Furthermore, leveraging the features of candidates in the form of query positional embedding results in the best performance, outperforming addition and concatenation operations by 0.4 AP and 0.2 AP, respectively.

Disappearance dynamic anchor queries. In Tab. 3f, we explore how to initialize the query feature embedding and positional embedding of disappearance DAQ. We find that initializing query feature of disappearance DAQ from the initial queries in the segmenter (as shown in Fig. 3) yields better AP than using a new shared learnable embedding for all disappearance DAQ (37.1 vs. 36.5). For generation of positional embedding of disappearance DAQ, we find utilizing the momentum-weighted appearance feature of tracked objects yield better AP than utilizing the query feature of tracked objects (37.1 vs. 36.8).

Emergence and disappearance simulation. We employ a threshold to filter out low-scoring tracked objects in emergence simulation. Tab. 3c illustrates the results when using different thresholds. A minimal threshold (0.01) results in insufficient new emergence cases, whereas a larger threshold (0.5) disrupts the model’s ability to learn continuous tracking. Both result in poor performance (34.2 AP and 33.2 AP). A similar phenomenon is observed in the disappearance

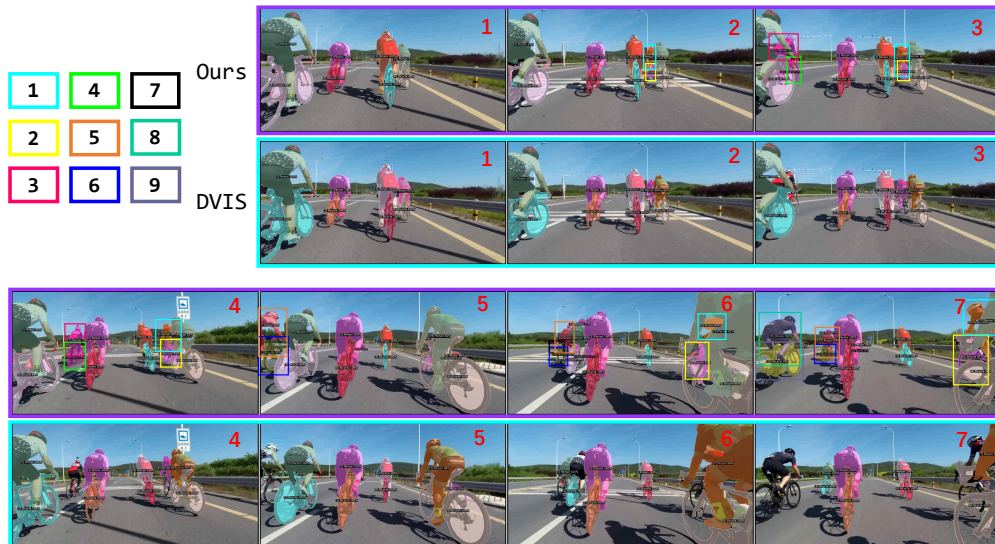


Fig. 7: Qualitative results comparison for emergence detection and disappearance filtering. The performance enhancements are highlighted by rectangles in various colors, each color representing an individual video object. It’s better to view with zooming in $8\times$.

simulation, as shown in Tab. 3d. The simulation of an object’s disappearance in a solitary frame within a video clip fails to generate sufficient disappearance cases. Conversely, simulating the disappearance across all frames compromises the model’s capability to learn continuous tracking. Consequently, we have determined that a threshold of 0.1 strikes an optimal balance for simulating emergence, and we opt for a stochastic selection of frames in a video clip to simulate disappearance. This strategy ensures ample emergence and disappearance cases while preserving the model’s tracking capability for continually appearing objects.

Qualitative results comparison. In Fig. 7, we present the visual comparison with our baseline. In this challenging scene, there are new-emerging, disappearing, and reappearing video objects. Our method accurately addresses all these scenarios, whereas DVIS suffers from issues including missed new-emerging objects and ID switches. Although DVIS detected object 1 in frame 2, it incorrectly switched the ID of another object to that of object 1. Regarding the reappearance of objects 1 and 2 in Frame 6, our method successfully maintained continuous tracking. In Frame 7, DVIS incorrectly switched the IDs of two nearby disappearing objects to objects 5 and 6, whereas our method correctly handled these disappearing cases.

5 Conclusion

We observed that current SOTA query-based video segmentation methods perform poorly on newly emerging and disappearing objects. We have analyzed and identified the significant transition gap hindering the network’s learning. We address this challenge by proposing dynamic anchor queries for shortening the

transition gap. We also introduce a query-level simulation strategy for simulating object disappearance and emergence without additional costs. By integrating our proposed dynamic anchor queries and simulation strategy into DVIS, we obtained DVIS-DAQ, which achieved SOTA performance on mainstream video segmentation benchmarks. Our research will inspire the video community to bridge the gap between current advancements in the standard benchmarks and real-world application requirements.

Limitations. We have significantly enhanced the capability of current query-based methods to handle newly emerging and disappearing objects. However, we introduced an additional tracker specifically to address object disappearance. While the additional computational cost is minimal, it undoubtedly introduces more hyperparameters. In the future, we will explore using a single model to effectively handle continuously appearing, newly emerging, and disappearing objects. Additionally, our model reaches its performance peak after 160k training iterations. Although this issue is prevalent in other methods, such as GenVIS and DVIS++, we believe there is ample room for optimization to enhance the model’s training efficiency.

References

1. Athar, A., Hermans, A., Luiten, J., Ramanan, D., Leibe, B.: Tarvis: A unified approach for target-based video segmentation. In: CVPR (2023) 4, 11
2. Athar, A., Mahadevan, S., Ošep, A., Leal-Taixé, L., Leibe, B.: Stem-seg: Spatio-temporal embeddings for instance segmentation in videos. In: ECCV (2020) 5
3. Bekuzarov, M., Bermudez, A., Lee, J.Y., Li, H.: Xmem++: Production-level video segmentation from few annotated frames (2023) 5
4. Bertasius, G., Torresani, L.: Classifying, segmenting, and tracking object instances in video with mask propagation (2022) 5
5. Bertasius, G., Wang, H., Torresani, L.: Is space-time attention all you need for video understanding? In: ICML (2021) 1
6. Bewley, A., Ge, Z., Ott, L., Ramos, F., Upcroft, B.: Simple online and realtime tracking. In: ICIIP (2016) 5
7. Caelles, S., Maninis, K., Pont-Tuset, J., Leal-Taixé, L., Cremers, D., Van Gool, L.: One-shot video object segmentation. In: CVPR (2017) 5
8. Carion, N., Massa, F., Synnaeve, G., Usunier, N., Kirillov, A., Zagoruyko, S.: End-to-end object detection with transformers. In: ECCV (2020) 4
9. Chen, Z., Duan, Y., Wang, W., He, J., Lu, T., Dai, J., Qiao, Y.: Vision transformer adapter for dense predictions. arXiv preprint arXiv:2205.08534 (2022) 10
10. Cheng, B., Choudhuri, A., Misra, I., Kirillov, A., Girdhar, R., Schwing, A.G.: Mask2former for video instance segmentation. arXiv preprint arXiv:2112.10764 (2021) 4, 5, 23
11. Cheng, B., Misra, I., Schwing, A.G., Kirillov, A., Girdhar, R.: Masked-attention mask transformer for universal image segmentation. In: CVPR (2022) 10
12. Cheng, B., Schwing, A., Kirillov, A.: Per-pixel classification is not all you need for semantic segmentation. NeurIPS (2021) 4
13. Cheng, H.K., Oh, S.W., Price, B., Schwing, A., Lee, J.Y.: Tracking anything with decoupled video segmentation. In: ICCV (2023) 4

14. Cheng, H.K., Tai, Y.W., Tang, C.K.: Rethinking space-time networks with improved memory coverage for efficient video object segmentation. In: NeurIPS (2021) [5](#)
15. Ding, H., Liu, C., He, S., Jiang, X., Torr, P.H., Bai, S.: MOSE: A new dataset for video object segmentation in complex scenes. In: ICCV (2023) [5](#)
16. Dosovitskiy, A., Beyer, L., Kolesnikov, A., Weissenborn, D., Zhai, X., Unterthiner, T., Dehghani, M., Minderer, M., Heigold, G., Gelly, S., et al.: An image is worth 16x16 words: Transformers for image recognition at scale. ICLR (2021) [4](#), [10](#), [11](#)
17. Gao, R., Wang, L.: MeMOTR: Long-term memory-augmented transformer for multi-object tracking. In: ICCV (2023) [5](#)
18. Hannan, T., Koner, R., Bernhard, M., Shit, S., Menze, B., Tresp, V., Schubert, M., Seidl, T.: Gratt-vis: Gated residual attention for auto rectifying video instance segmentation. arXiv preprint arXiv:2305.17096 (2023) [1](#), [4](#)
19. He, J., Yu, Q., Shin, I., Deng, X., Shen, X., Yuille, A., Chen, L.C.: Maxtron: Mask transformer with trajectory attention for video panoptic segmentation (2023) [5](#)
20. He, K., Zhang, X., Ren, S., Sun, J.: Deep residual learning for image recognition. In: CVPR (2016) [11](#)
21. Heo, M., Hwang, S., Hyun, J., Kim, H., Oh, S.W., Lee, J.Y., Kim, S.J.: A generalized framework for video instance segmentation. In: CVPR (2023) [1](#), [2](#), [4](#), [5](#), [8](#), [10](#), [20](#), [21](#)
22. Heo, M., Hwang, S., Oh, S.W., Lee, J.Y., Kim, S.J.: Vita: Video instance segmentation via object token association. NIPS (2022) [4](#)
23. Huang, D.A., Yu, Z., Anandkumar, A.: Minvis: A minimal video instance segmentation framework without video-based training. NeurIPS (2022) [1](#), [2](#), [4](#), [5](#), [10](#), [11](#), [20](#)
24. Kim, D., Woo, S., Lee, J.Y., Kweon, I.S.: Video panoptic segmentation. In: CVPR (2020) [1](#), [4](#), [5](#), [11](#)
25. Kim, D., Woo, S., Lee, J.Y., Kweon, I.S.: Video panoptic segmentation. In: CVPR (2020) [5](#)
26. Kim, D., Xie, J., Wang, H., Qiao, S., Yu, Q., Kim, H.S., Adam, H., Kweon, I.S., Chen, L.C.: Tubeformer-deeplab: Video mask transformer. In: CVPR (2022) [4](#)
27. Leal-Taixé, L., Canton-Ferrer, C., Schindler, K.: Learning by tracking: Siamese cnn for robust target association. In: CVPR Workshops (2016) [5](#)
28. Li, J., Yu, B., Rao, Y., Zhou, J., Lu, J.: Tcovis: Temporally consistent online video instance segmentation. In: ICCV (2023) [1](#), [4](#)
29. Li, M., Li, S., Zhang, X., Zhang, L.: Univs: Unified and universal video segmentation with prompts as queries (2024) [5](#)
30. Li, X., Ding, H., Zhang, W., Yuan, H., Cheng, G., Jiangmiao, P., Chen, K., Liu, Z., Loy, C.C.: Transformer-based visual segmentation: A survey. arXiv pre-print (2023) [4](#)
31. Li, X., Xu, S., Cheng, Y.Y., Tong, Y., Tao, D., et al.: Panoptic-partformer: Learning a unified model for panoptic part segmentation. ECCV (2022) [4](#)
32. Li, X., Yuan, H., Li, W., Ding, H., Wu, S., Zhang, W., Li, Y., Chen, K., Loy, C.C.: Omg-seg: Is one model good enough for all segmentation? CVPR (2024) [5](#)
33. Li, X., Yuan, H., Zhang, W., Cheng, G., Pang, J., Loy, C.C.: Tube-link: A flexible cross tube framework for universal video segmentation. In: ICCV (2023) [1](#), [4](#), [5](#)
34. Li, X., Zhang, W., Pang, J., Chen, K., Cheng, G., Tong, Y., Loy, C.C.: Video k-net: A simple, strong, and unified baseline for video segmentation. In: CVPR (2022) [4](#)
35. Lin, C.C., Hung, Y., Feris, R., He, L.: Video instance segmentation tracking with a modified vae architecture. In: CVPR (2020) [4](#)

36. Liu, Z., Lin, Y., Cao, Y., Hu, H., Wei, Y., Zhang, Z., Lin, S., Guo, B.: Swin transformer: Hierarchical vision transformer using shifted windows. In: ICCV (2021) [11](#)
37. Meinhardt, T., Feiszli, M., Fan, Y., Leal-Taixe, L., Ranjan, R.: Novis: A case for end-to-end near-online video instance segmentation. arXiv preprint arXiv:2308.15266 (2023) [4](#)
38. Meinhardt, T., Kirillov, A., Leal-Taixe, L., Feichtenhofer, C.: Trackformer: Multi-object tracking with transformers. In: CVPR (2022) [5](#)
39. Miao, J., Wang, X., Wu, Y., Li, W., Zhang, X., Wei, Y., Yang, Y.: Large-scale video panoptic segmentation in the wild: A benchmark. In: CVPR (2022) [4](#), [6](#), [10](#), [11](#)
40. Miao, J., Wei, Y., Wu, Y., Liang, C., Li, G., Yang, Y.: Vspw: A large-scale dataset for video scene parsing in the wild. In: CVPR (2021) [4](#)
41. Oquab, M., Darcet, T., Moutakanni, T., Vo, H., Szafraniec, M., Khalidov, V., Fernandez, P., Haziza, D., Massa, F., El-Nouby, A., et al.: Dinov2: Learning robust visual features without supervision. arXiv preprint arXiv:2304.07193 (2023) [10](#)
42. Pang, J., Qiu, L., Li, X., Chen, H., Li, Q., Darrell, T., Yu, F.: Quasi-dense similarity learning for multiple object tracking. In: CVPR (2021) [5](#)
43. Pang, Z., Li, Z., Wang, N.: Simpletrack: Understanding and rethinking 3d multi-object tracking. arXiv preprint arXiv:2111.09621 (2021) [5](#)
44. Park, K., Woo, S., Oh, S.W., Kweon, I.S., Lee, J.Y.: Per-clip video object segmentation. In: CVPR (2022) [5](#)
45. Patrick, M., Campbell, D., Asano, Y.M., Metzger, I.M.F., Feichtenhofer, C., Vedaldi, A., Henriques, J.F.: Keeping your eye on the ball: Trajectory attention in video transformers. In: NeurIPS (2021) [1](#)
46. Porzi, L., Hofinger, M., Ruiz, I., Serrat, J., Buló, S.R., Kotschieder, P.: Learning multi-object tracking and segmentation from automatic annotations. In: CVPR (2020) [5](#)
47. Qi, J., Gao, Y., Hu, Y., Wang, X., Liu, X., Bai, X., Belongie, S., Yuille, A., Torr, P.H., Bai, S.: Occluded video instance segmentation: A benchmark. IJCV (2022) [1](#), [6](#), [10](#), [20](#)
48. Qiao, S., Zhu, Y., Adam, H., Yuille, A., Chen, L.C.: Vip-deeplab: Learning visual perception with depth-aware video panoptic segmentation. In: CVPR (2021) [4](#)
49. Sanghyun, W., Kwanyong, P., Seoung, W.O., In, S.K., Joon-Young, L.: Tracking by associating clips. In: ECCV (2022) [5](#)
50. Seong, H., Oh, S.W., Lee, J.Y., Lee, S., Lee, S., Kim, E.: Hierarchical memory matching network for video object segmentation. In: Proceedings of the IEEE/CVF International Conference on Computer Vision (2021) [5](#)
51. Sun, P., Cao, J., Jiang, Y., Yuan, Z., Bai, S., Kitani, K., Luo, P.: Dancetrack: Multi-object tracking in uniform appearance and diverse motion. arXiv preprint arXiv:2111.14690 (2021) [5](#)
52. Sun, P., Cao, J., Jiang, Y., Zhang, R., Xie, E., Yuan, Z., Wang, C., Luo, P.: Transtrack: Multiple-object tracking with transformer. arXiv preprint arXiv:2012.15460 (2020) [5](#)
53. Wang, X., Girdhar, R., Yu, S.X., Misra, I.: Cut and learn for unsupervised object detection and instance segmentation. In: CVPR (2023) [4](#)
54. Wang, Y., Xu, Z., Wang, X., Shen, C., Cheng, B., Shen, H., Xia, H.: End-to-end video instance segmentation with transformers. In: CVPR (2021) [4](#)
55. Weber, M., Xie, J., Collins, M., Zhu, Y., Voigtlaender, P., Adam, H., Green, B., Geiger, A., Leibe, B., Cremers, D., et al.: Step: Segmenting and tracking every pixel. arXiv preprint arXiv:2102.11859 (2021) [4](#)

56. Weng, Y., Han, M., He, H., Li, M., Yao, L., Chang, X., Zhuang, B.: Mask propagation for efficient video semantic segmentation. arXiv preprint arXiv:2310.18954 (2023) [4](#)
57. Wu, J., Cao, J., Song, L., Wang, Y., Yang, M., Yuan, J.: Track to detect and segment: An online multi-object tracker. In: CVPR (2021) [5](#)
58. Wu, J., Li, X., Xu, S., Yuan, H., Ding, H., Yang, Y., Li, X., Zhang, J., Tong, Y., Jiang, X., Ghanem, B., Tao, D.: Towards open vocabulary learning: A survey. T-PAMI (2024) [4](#)
59. Wu, J., Jiang, Y., Bai, S., Zhang, W., Bai, X.: Seqformer: Sequential transformer for video instance segmentation. In: ECCV (2022) [4](#)
60. Wu, J., Liu, Q., Jiang, Y., Bai, S., Yuille, A., Bai, X.: In defense of online models for video instance segmentation. In: ECCV (2022) [1](#), [4](#), [5](#)
61. Xu, J., Cao, Y., Zhang, Z., Hu, H.: Spatial-temporal relation networks for multi-object tracking. In: ICCV (2019) [5](#)
62. Xu, S., Yuan, H., Shi, Q., Qi, L., Wang, J., Yang, Y., Li, Y., Chen, K., Tong, Y., Ghanem, B., Li, X., Yang, M.H.: Rap-sam:towards real-time all-purpose segment anything. arXiv preprint (2024) [5](#)
63. Yan, B., Jiang, Y., Sun, P., Wang, D., Yuan, Z., Luo, P., Lu, H.: Towards grand unification of object tracking. In: ECCV (2022) [5](#)
64. Yan, B., Jiang, Y., Wu, J., Wang, D., Luo, P., Yuan, Z., Lu, H.: Universal instance perception as object discovery and retrieval. In: CVPR (2023) [4](#)
65. Yang, J., Peng, W., Li, X., Guo, Z., Chen, L., Li, B., Ma, Z., Zhou, K., Zhang, W., Loy, C.C., et al.: Panoptic video scene graph generation. In: CVPR (2023) [1](#)
66. Yang, L., Fan, Y., Xu, N.: Video instance segmentation. In: ICCV (2019) [1](#), [4](#), [6](#), [10](#)
67. Yang, S., Fang, Y., Wang, X., Li, Y., Fang, C., Shan, Y., Feng, B., Liu, W.: Crossover learning for fast online video instance segmentation. In: ICCV (2021) [4](#)
68. Ying, K., Zhong, Q., Mao, W., Wang, Z., Chen, H., Wu, L.Y., Liu, Y., Fan, C., Zhuge, Y., Shen, C.: Ctvis: Consistent training for online video instance segmentation. In: ICCV (2023) [1](#), [4](#), [5](#), [7](#), [10](#)
69. Yu, F., Chen, H., Wang, X., Xian, W., Chen, Y., Liu, F., Madhavan, V., Darrell, T.: Bdd100k: A diverse driving dataset for heterogeneous multitask learning. In: CVPR (2020) [2](#)
70. Zeng, F., Dong, B., Zhang, Y., Wang, T., Zhang, X., Wei, Y.: Motr: End-to-end multiple-object tracking with transformer. In: ECCV (2022) [5](#)
71. Zhang, T., Tian, X., Wu, Y., Ji, S., Wang, X., Zhang, Y., Wan, P.: Dvis: Decoupled video instance segmentation framework. In: ICCV (2023) [1](#), [2](#), [3](#), [4](#), [5](#), [8](#), [9](#), [10](#), [11](#), [12](#), [13](#), [21](#), [22](#)
72. Zhang, T., Tian, X., Zhou, Y., Ji, S., Wang, X., Tao, X., Zhang, Y., Wan, P., Wang, Z., Wu, Y.: Dvis++: Improved decoupled framework for universal video segmentation. arXiv preprint arXiv:2312.13305 (2023) [1](#), [2](#), [5](#), [9](#), [10](#), [11](#), [12](#)
73. Zhang, W., Pang, J., Chen, K., Loy, C.C.: K-net: Towards unified image segmentation. NIPS (2021) [4](#)
74. Zhang, Y., Sun, P., Jiang, Y., Yu, D., Weng, F., Yuan, Z., Luo, P., Liu, W., Wang, X.: Bytetrack: Multi-object tracking by associating every detection box. ECCV (2022) [5](#)
75. Zhou, Q., Li, X., He, L., Yang, Y., Cheng, G., Tong, Y., Ma, L., Tao, D.: Transvod: end-to-end video object detection with spatial-temporal transformers. T-PAMI (2022) [5](#)

76. Zhou, Y., Zhang, H., Lee, H., Sun, S., Li, P., Zhu, Y., Yoo, B., Qi, X., Han, J.J.: Slot-vps: Object-centric representation learning for video panoptic segmentation. In: CVPR (2022) 5
77. Zhu, J., Yang, H., Liu, N., Kim, M., Zhang, W., Yang, M.H.: Online multi-object tracking with dual matching attention networks. In: ECCV (2018) 5
78. Zhu, X., Xiong, Y., Dai, J., Yuan, L., Wei, Y.: Deep feature flow for video recognition. CVPR (2016) 4

A Appendix

Overview. In this section, we first introduce more implementation details and training settings of our model. To further substantiate the generalizability and effectiveness of our DAQ design, we integrate the DAQ into an alternative video segmentation framework, GenVIS [21], and conduct experiments on the OVIS [47] dataset. Additionally, we provide more ablation studies to verify the effectiveness of the detailed components of the DAQ design. Lastly, we present a collection of qualitative results and supplementary video files to demonstrate the full performance of our method in challenging scenes.

.1 More Implementation Details

Spatio-temporal padding. The tracker incorporating with DAQ outputs N_{trc} video objects for a video with T frames, denoted as $\{\{Q^i\}_{t_i}^{T_i}\}_{i=1}^{N_{trc}}$, where the temporal dimension lengths $(T_i - t_i + 1)$ of these N_{trc} video objects may vary. Therefore, before feeding into the temporal refiner, we pad each video object sequence with the momentum-weighted appearance feature at the time steps $t \in \{1, \dots, t_i - 1, T_i + 1, \dots, T\}$, where the video object does not appear. The padded results are denoted as $\{\{Q^i\}_1^T\}_{i=1}^{N_{trc}}$. In addition to temporal padding, we also perform padding in the spatial dimension. We first use the Hungarian algorithm to naively extract N video object feature sequences $\{\{Q_{naive}^i\}_1^T\}_{i=1}^N$ from the object queries $Q_{Seg} \in R^{N \times C}$ of all frames, as MinVIS [23] does. Then, we select the top $N - N_{trc}$ video objects based on classification scores to pad $\{\{Q^i\}_1^T\}_{i=1}^{N_{trc}}$ in the spatial dimension to obtain $\{\{Q^i\}_1^T\}_{i=1}^N$.

Training details. We employ the AdamW optimizer with an initial learning rate of 1e-4 and a weight decay of 5e-2 for training. For the VIS task, we use the COCO joint training setting to train the model. For the VPS task, no additional datasets are employed. When training in offline mode, we freeze all modules except the temporal refiner and initialize these modules with parameters trained in online mode. We set the lengths of training video clips as 5 and 15 for online and offline modes, respectively. For all datasets, we train for 160K iterations and apply learning rate decay at 112K iterations.

.2 Additional Experiments

Generalization ability of DAQ. To further substantiate the efficacy of the Dynamic Attention Query (DAQ), we integrated it into an alternative video segmentation framework, GenVIS [21], culminating in the development of an augmented architecture dubbed GenVIS-DAQ. We employed ResNet-50 as the backbone and conducted experiments on the more challenging OVIS dataset. For a fair comparison, we used GenVIS without the instance prototype memory (IPM) as our baseline and adhered to the original training strategies utilized by GenVIS. The results are reported in Tab. A1. By incorporating DAQ, we achieved an improvement of 1.7 AP for GenVIS. This demonstrates that using DAQ to

manage the emergence and disappearance of objects in videos can enhance the capability of query-based video segmentation methods to handle complex scenes.

Performance improvements on emergence and disappearance. We conduct separate evaluations for newly emerged and disappeared objects on the OVIS and VIPSeg datasets, with the results presented in Tab .A2. For newly emerged and disappeared objects, our method outperforms the baseline DVIS [71] by 7.3 VPQ and 6.8 AP on VIPSeg and OVIS, respectively, indicating the effectiveness of our method for this problem.

Feature transition gap. We claimed that our DAQ mechanism enhances the management of objects’ emergence and disappearance by shortening the feature transition gap between the anchor query and the target. We define the transition gap as the feature distance from the anchor query to the target. In DVIS [71], the anchor query for a newly emerged object is a background query, and the target is the feature representation of the object. In contrast, the anchor query for a disappeared object is the feature representation of the object before it disappeared, and the target is a background feature. In our method, the dynamic anchor query is a mixture of background and foreground for both situations, where learnable embeddings and candidates provide the background and foreground features, respectively. Our DAQs offer information on potential future states of targets. Therefore, our method results in a smaller transition gap to the target. As shown in Tab. A3, we calculate the transition gap for DVIS and our method, where our DAQ significantly shortens the transition gap.

Table A1: Results on the validation sets of OVIS.

Method	OVIS				
	AP	AP ₅₀	AP ₇₅	AR ₁	AR ₁₀
Baseline	34.8	59.0	35.4	17.0	39.0
GenVIS [21] + DAQ	36.5 (+1.7)	64.5 (+5.5)	35.6 (+0.2)	15.4 (-1.6)	42.5 (+3.5)

Table A2: Performance improvements. VPQ^{all} and AP^{all} represent performance on all objects, while VPQ^{ed} and AP^{ed} for emerging and disappearing objects.

Method	VIPSeg		OVIS	
	VPQ ^{all}	VPQ ^{ed}	AP ^{all}	AP ^{ed}
DVIS [71]	38.7	29.0	26.9	19.1
DVIS+DAQ	42.1	36.3	30.2	25.9
Improvement	+3.4	+7.3	+3.3	+6.8

Table A3: Feature transition gap. CS denotes Cosine Similarity. NED denotes Normalized Euclidean Distance. Symbols \uparrow and \downarrow denote “larger is better” and “smaller is better”, respectively.

Methods	CS \uparrow	NED \downarrow
DVIS [71]	0.08 ± 0.06	0.68 ± 0.02
DVIS+DAQ	0.32 ± 0.08	0.59 ± 0.04

.3 More Ablation Studies

Softmax in the disappearance tracker. As depicted in Tab. A4a, compared to the standard cross-attention, which applies SoftMax on the key dimension, we observe that applying SoftMax on the query dimension yields better performance. This is because employing SoftMax on the query dimension prevents different disappearance DAQ from merging the features of the same candidate into the same target query.

Spatio-temporal padding. As shown in Tab. A4c, before integrating online results into the offline module, it is imperative to apply both temporal and spatial padding. This preparatory step guarantees that the input is appropriately aligned in both time and space to fulfill the requirement of the offline module. Opting to pad with momentum-weighted appearance features rather than zero or learnable padding affords the advantage of tailoring feature information to each individual video object. This tailored padding strategy has been instrumental in achieving a notable improvement in AP (42.7 vs. 38.4). Additionally, performing spatial padding subsequent to temporal padding can further enhance the AP (43.5 vs. 42.7).

Computation cost analysis. The computational cost of DVIS-DAQ components was measured by evaluating the parameters, FLOPs, and inference time of the segmenter and tracker with DAQ. Tab. As shown in Tab. A4b, the additional tracker #2 only accounts for 1.6% of the total computational cost.

.4 More Qualitative Results

Fig. A1 presents qualitative results in complex scenes. To fully demonstrate the performance of our method in challenging scenes such as fast motion and occlusions, we also provide supplementary videos for reference.

Table A4: More ablation studies on our proposed DAQ and other network details.

(a) The ablation study of the softmax dimension of cross-attention in disappearance tracker. (b) Computational cost. Segmenter is implemented by Mask2Former [10] with ResNet-50 as backbone. Input frames are resized to 480p.

Dimension	AP
K-dim	36.6
Q-dim	37.1

Component	Params (M)	FLOPs (G)	Time (ms)
Segmenter	44.15	225.14	50.01
Tracker #1	9.94	3.78	10.32
Tracker #2	8.68	3.67	

(c) Padding the online output queries to offline inputs. For temporal padding, *None* denotes using attention masks in the offline module instead of padding; *Zero*, *Learn*, and *AppF* denote padding with zero value, a learnable embedding, and the momentum-weighted appearance feature, respectively. For spatial padding, *No* denotes not to pad, and *Yes* denotes padding with naively associated video objects.

Metric	None	Temporal			Spatial	
		Zero	Learn	AppF	No	Yes
AP	38.4	39.0	39.1	42.7	42.7	43.5

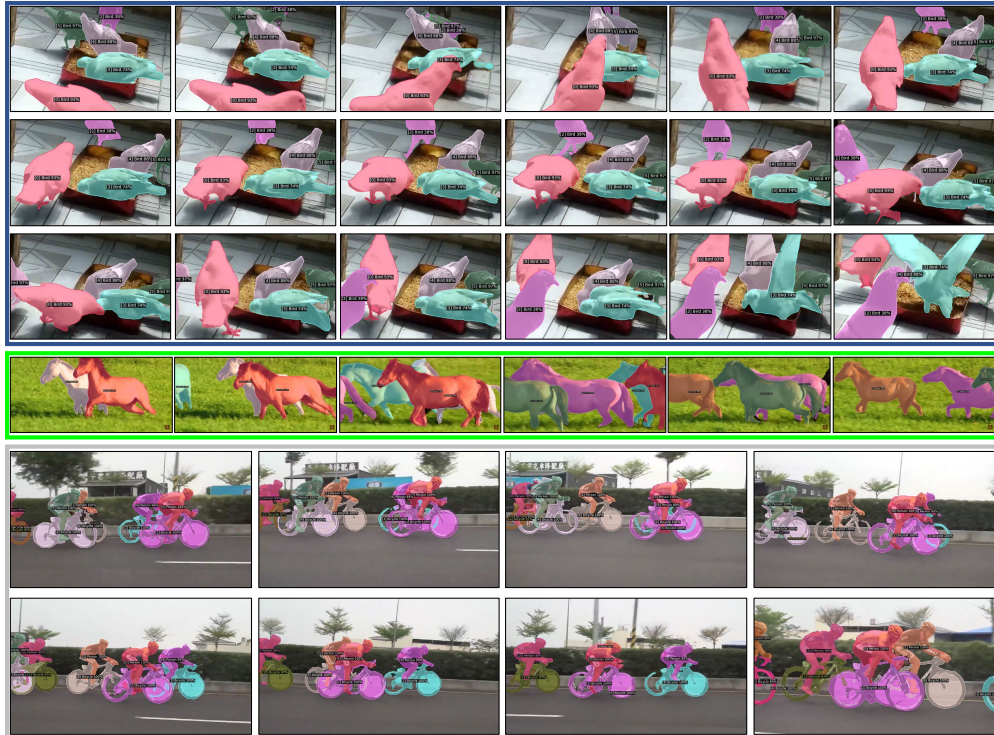


Fig. A1: Qualitative results. It's better to view with zooming in $8\times$.

Improving Video Segmentation via Dynamic Anchor Queries

Anonymous ECCV 2024 Submission

Paper ID #6733

A Appendix

Overview. In this section, we first introduce more implementation details and training settings of our model. To further substantiate the generalizability and effectiveness of our DAQ design, we integrate the DAQ into an alternative video segmentation framework, GenVIS [?], and conduct experiments on the OVIS [?] dataset. Additionally, we provide more ablation studies to verify the effectiveness of the detailed components of the DAQ design. Lastly, we present a collection of qualitative results and supplementary video files to demonstrate the full performance of our method in challenging scenes.

3.1 More Implementation Details

Spatio-temporal padding. The tracker incorporating with DAQ outputs N_{trc} video objects for a video with T frames, denoted as $\{\{Q^i\}_{t_i}^{T_i}\}_{i=1}^{N_{trc}}$, where the temporal dimension lengths $(T_i - t_i + 1)$ of these N_{trc} video objects may vary. Therefore, before feeding into the temporal refiner, we pad each video object sequence with the momentum-weighted appearance feature at the time steps $t \in \{1, \dots, t_i - 1, T_i + 1, \dots, T\}$, where the video object does not appear. The padded results are denoted as $\{\{Q^i\}_1^T\}_{i=1}^{N_{trc}}$. In addition to temporal padding, we also perform padding in the spatial dimension. We first use the Hungarian algorithm to naively extract N video object feature sequences $\{\{Q_{naive}^i\}_1^T\}_{i=1}^N$ from the object queries $Q_{Seg} \in R^{N \times C}$ of all frames, as MinVIS [?] does. Then, we select the top $N - N_{trc}$ video objects based on classification scores to pad $\{\{Q^i\}_1^T\}_{i=1}^{N_{trc}}$ in the spatial dimension to obtain $\{\{Q^i\}_1^T\}_{i=1}^N$.

Training details. We employ the AdamW optimizer with an initial learning rate of 1e-4 and a weight decay of 5e-2 for training. For the VIS task, we use the COCO joint training setting to train the model. For the VPS task, no additional datasets are employed. When training in offline mode, we freeze all modules except the temporal refiner and initialize these modules with parameters trained in online mode. We set the lengths of training video clips as 5 and 15 for online and offline modes, respectively. For all datasets, we train for 160K iterations and apply learning rate decay at 112K iterations.

035 .2 Additional Experiments 035

036 **Generalization ability of DAQ.** To further substantiate the efficacy of the 036
 037 Dynamic Attention Query (DAQ), we integrated it into an alternative video seg- 037
 038 mentation framework, GenVIS [?], culminating in the development of an aug- 038
 039 mented architecture dubbed GenVIS-DAQ. We employed ResNet-50 as the back- 039
 040 bone and conducted experiments on the more challenging OVIS dataset. For a 040
 041 fair comparison, we used GenVIS without the instance prototype memory (IPM) 041
 042 as our baseline and adhered to the original training strategies utilized by Gen- 042
 043 VIS. The results are reported in Tab. A1. By incorporating DAQ, we achieved 043
 044 an improvement of 1.7 AP for GenVIS. This demonstrates that using DAQ to 044
 045 manage the emergence and disappearance of objects in videos can enhance the 045
 046 capability of query-based video segmentation methods to handle complex scenes. 046

047 **Performance improvements on emergence and disappearance.** We con- 047
 048 duct separate evaluations for newly emerged and disappeared objects on the 048
 049 OVIS and VIPSeg datasets, with the results presented in Tab .A2. For newly 049
 050 emerged and disappeared objects, our method outperforms the baseline DVIS [?] 050
 051 by 7.3 VPQ and 6.8 AP on VIPSeg and OVIS, respectively, indicating the effec- 051
 052 tiveness of our method for this problem. 052

053 **Feature transition gap.** We claimed that our DAQ mechanism enhances the 053
 054 management of objects’ emergence and disappearance by shortening the feature 054
 055 transition gap between the anchor query and the target. We define the transition 055
 056 gap as the feature distance from the anchor query to the target. In DVIS [?], 056
 057 the anchor query for a newly emerged object is a background query, and the 057
 058 target is the feature representation of the object. In contrast, the anchor query 058
 059 for a disappeared object is the feature representation of the object before it dis- 059
 060 appeared, and the target is a background feature. In our method, the dynamic 060
 061 anchor query is a mixture of background and foreground for both situations, 061
 062 where learnable embeddings and candidates provide the background and fore- 062
 063 ground features, respectively. Our DAQs offer information on potential future 063
 064 states of targets. Therefore, our method results in a smaller transition gap to 064
 065 the target. As shown in Tab. A3, we calculate the transition gap for DVIS and 065
 066 our method, where our DAQ significantly shortens the transition gap. 066

Table A1: Results on the validation sets of OVIS.

Method	OVIS				
	AP	AP ₅₀	AP ₇₅	AR ₁	AR ₁₀
Baseline	34.8	59.0	35.4	17.0	39.0
GenVIS [?] + DAQ	36.5 (+1.7)	64.5 (+5.5)	35.6 (+0.2)	15.4 (-1.6)	42.5 (+3.5)

Table A2: Performance improvements. VPQ^{all} and AP^{all} represent performance on all objects, while VPQ^{ed} and AP^{ed} for emerging and disappearing objects.

Method	VIPSeg		OVIS	
	VPQ^{all}	VPQ^{ed}	AP^{all}	AP^{ed}
DVIS [?]	38.7	29.0	26.9	19.1
DVIS+DAQ	42.1	36.3	30.2	25.9
Improvement	+3.4	+7.3	+3.3	+6.8

Table A3: Feature transition gap. CS denotes Cosine Similarity. NED denotes Normalized Euclidean Distance. Symbols \uparrow and \downarrow denote “larger is better” and “smaller is better”, respectively.

Methods	CS \uparrow	NED \downarrow
DVIS [?]	0.08 ± 0.06	0.68 ± 0.02
DVIS+DAQ	0.32 ± 0.08	0.59 ± 0.04

067 .3 More Ablation Studies 067

068 **Softmax in the disappearance tracker.** As depicted in Tab. A4a, compared 068
 069 to the standard cross-attention, which applies SoftMax on the key dimension, 069
 070 we observe that applying SoftMax on the query dimension yields better per- 070
 071 formance. This is because employing SoftMax on the query dimension prevents 071
 072 different disappearance DAQ from merging the features of the same candidate 072
 073 into the same target query. 073

074 **Spatio-temporal padding.** As shown in Tab. A4c, before integrating online 074
 075 results into the offline module, it is imperative to apply both temporal and 075
 076 spatial padding. This preparatory step guarantees that the input is appropriately 076
 077 aligned in both time and space to fulfill the requirement of the offline module. 077
 078 Opting to pad with momentum-weighted appearance features rather than zero or 078
 079 learnable padding affords the advantage of tailoring feature information to each 079
 080 individual video object. This tailored padding strategy has been instrumental in 080
 081 achieving a notable improvement in AP (42.7 vs. 38.4). Additionally, performing 081
 082 spatial padding subsequent to temporal padding can further enhance the AP 082
 083 (43.5 vs. 42.7). 083

084 **Computation cost analysis.** The computational cost of DVIS-DAQ compo- 084
 085 nents was measured by evaluating the parameters, FLOPs, and inference time of 085
 086 the segmenter and tracker with DAQ. Tab. As shown in Tab. A4b, the additional 086
 087 tracker #2 only accounts for 1.6% of the total computational cost. 087

088 .4 More Qualitative Results 088

089 Fig. A1 presents qualitative results in complex scenes. To fully demonstrate 089
 090 the performance of our method in challenging scenes such as fast motion and 090
 091 occlusions, we also provide supplementary videos for reference. 091

Table A4: More ablation studies on our proposed DAQ and other network details.

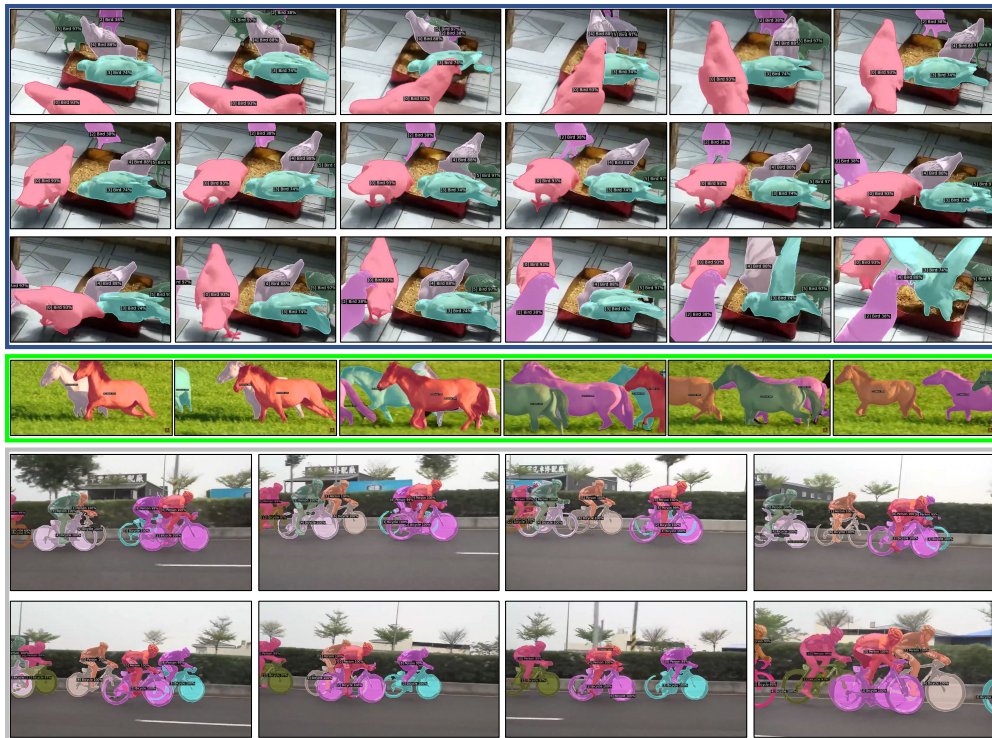
(a) The ablation study of the softmax dimension of cross-attention in disappearance tracker. (b) Computational cost. Segmenter is implemented by Mask2Former [?] with ResNet-50 as backbone. Input frames are resized to 480p.

Dimension	AP
K-dim	36.6
Q-dim	37.1

Component	Params (M)	FLOPs (G)	Time (ms)
Segmenter	44.15	225.14	50.01
Tracker #1	9.94	3.78	10.32
Tracker #2	8.68	3.67	

(c) Padding the online output queries to offline inputs. For temporal padding, *None* denotes using attention masks in the offline module instead of padding; *Zero*, *Learn*, and *AppF* denote padding with zero value, a learnable embedding, and the momentum-weighted appearance feature, respectively. For spatial padding, *No* denotes not to pad, and *Yes* denotes padding with naively associated video objects.

Metric	None	Temporal			Spatial	
		Zero	Learn	AppF	No	Yes
AP	38.4	39.0	39.1	42.7	42.7	43.5

**Fig. A1:** Qualitative results. It's better to view with zooming in $8\times$.